Dendrochronologia 29 (2011) 201–210

Contents lists available at ScienceDirect

Dendrochronologia

journal homepage: www.elsevier.de/dendro

Original article

Cross-sectional interpolation of annual rings within a 3D root model

B. Wagner[a,b,*], H. Gärtner[a], S. Santini[c], H. Ingensand[b]

[a] Swiss Federal Research Institute WSL, Zürcherstrasse 111, 8903 Birmensdorf, Switzerland
[b] Institute of Geodesy and Photogrammetry, ETH Zurich, 8093 Zurich, Switzerland
[c] Institute for Pervasive Computing, ETH Zurich, 8092 Zurich, Switzerland

ARTICLE INFO

Article history:
Received 22 June 2010
Accepted 13 December 2010

Keywords:
Laser scanning
3D modelling
Tree rings
Biomass
Ring boundaries

ABSTRACT

Ring width of a given year can be highly variable throughout the cross section of a stem. This is especially true for roots. Therefore, the entire circumference of tree rings is often needed for studies focusing on specific reactions of individual trees on certain environmental conditions. Also, ring reconstructions are of interest for biomass calculations estimated by the cross-sectional area. The aim of the study is thus to reconstruct tree rings of cross sections within a 3D root-surface model, which will be the basis for an upcoming 3D root-development model. A FARO ScanArm was used for the acquisition of the 3D root structure (Technologies Inc., 2010). Afterwards ring-width data was measured along 4 radii per cross section and the resulting ring boundaries were integrated into the 3D root model. A weighted interpolation algorithm was used to reconstruct entire ring-width profiles of the cross sections. The algorithm considered the ring-width variations of the adjacent radii as well as the outer shape of the cross section. Hence, the intention was to estimate ring width around the root circumference using ring widths measured along 4 radii and the surface dimensions of roots. Interpolated ring-width data was compared to the measured tree-ring data as a control for the developed interpolation algorithm. Comparisons between modelled and empirical values showed a mean absolute error of about 0.06 mm deviation, and with a few exceptions the growth patterns could be accurately simulated. This has permitted additional radii measurements to be replaced by model interpolations.

1. Introduction

Annual rings in trees and shrubs are important archives of past environmental conditions (Schweingruber, 2007). For this, measurements of various ring parameters as ring width or maximum latewood density are widely used for analyzing, e.g., the growth dynamics or climate conditions of the past. It is common practice in dendrochronological studies to take two cores per tree (Speer, 2010), which in many cases is sufficient for general analyses or for detecting the expressed population signal (Wigley et al., 1984). Although this method is widely accepted to efficiently represent the general growth development of the stem, tree-ring structures are often highly variable within cross sections and along tree stems. Due to this, analyzing entire cross sections showing the circumference of all tree rings would shed light on the detailed growing conditions of single tree stems. This is especially true for the potential analyses of the more complex growth development of entire tree-root systems (Danjon and Reubens, 2008; Heuret et al., 2006). Root systems influence the growth of the stem, but it is still unknown to what extent.

Dendrochronological studies focusing on roots are mostly concentrated on single roots, and hence, consider only punctual information related to the heterogeneous architecture of the entire coarse-root system. The heterogeneity of root systems is an expression of their sensitivity to the growing conditions such as mechanical stresses (Mattheck and Breloer, 1995). Detailed analyses of the growth development of an entire root system would help to identify and understand specific variations and relate these characteristics to the above-ground parts, especially the stems of trees. But due to the heterogeneity of root systems, analyzing one or two radii of single roots is not sufficient for a detailed reconstruction of their development. Here, the reconstruction of entire ring structures, which has been a concern in dendrochronology in relation to stems for some time (Entacher et al., 2007), plays a decisive role.

The approaches and study purposes for reconstructing entire tree-ring profiles are diverse. Data representing ring area (basal area increment), providing a better index of stem wood production than ring-width data (Le Blanc, 1990), are used for individual tree-growth models and yield equations.

* Corresponding author at: Swiss Federal Research Institute WSL, Zürcherstrasse 111, 8903 Birmensdorf, Switzerland. Tel.: +41 447392213; fax: +41 447392215.
E-mail address: bettina.wagner@wsl.ch (B. Wagner).

1125-7865/$ – see front matter
doi:10.1016/j.dendro.2010.12.003

Skatter (1998) described the outer shape of logs on bark, the outermost ring boundary and the borderline between heartwood and sapwood by using an arbitrary oriented ellipse derived by solving least square equations. Several other studies have aimed at reconstructing either the outer circumference of boles or tree rings by making cyclic or elliptical approximations of the rings or bole circumferences (Bindzi et al., 1996; Saint-André, 1998; Skatter, 1998; Skatter and Høibø, 1998; Saint-André and Leban, 2000; Ikami et al., 2008).

Linear interpolation between 36 radii was used by Saint-André and Leban (2000) to reconstruct the circumference of tree rings. This interpolation can be seen as a realistic approximation of the real tree-ring structures. However, the main drawback is the time required for measurements and calculations, especially with an increasing number of cross sections. Nevertheless, the approach was implemented to reconstruct an entire cross section and to record the entire circumference of the rings. Lewis (1997) simply used a sonic digitizer to reconstruct the ring's circumferences. Every 5th ring was digitized, which is also an immense workload and might not be applicable on a broader scale.

Overall, tree-ring reconstruction studies including wood asymmetry and wood properties are difficult to carry out due to the high number of radii required to estimate possible eccentricity and ellipticity of rings (Saint-André and Leban, 2000).

More recent studies have used image processing approaches such as edge detection algorithms to try to detect ring structures within images of tree cores (Conner et al., 1998, 2000; He et al., 2008) or entire cross sections (Cerda et al., 2007; von Arx and Dietz, 2005). Ring structures have been detected directly from images using edge detection algorithms (Soille and Misson, 2001; Laggoune et al., 2005; Cerda et al., 2007). The motivation is mainly to reduce the amount of work (Laggoune et al., 2005) and to get a realistic circumference structure of rings within a cross section.

However, these techniques often contain errors and no truly automated techniques exist (Laggoune et al., 2005). Even when good results are achieved, there are inherent problems. Typical problems (e.g., undetected ring boundaries or false rings) occur most likely when rings are narrow and species with low contrast between early and late wood are used. Cerda et al. (2007) used an edge-detection algorithm, which considers the bark shape of the cross-sectional image as a ring-approximation. The results were promising and the procedure might be applicable in future works on a broader scale. Related applications with similar techniques were used by Fablet and Le Josse (2005) who detected ring structures from otolith images of fish to estimate their age.

Further, there have been first attempts to reconstruct automated tree-ring profiles from computer tomography (CT) images (Entacher et al., 2007; Longuetaud et al., 2007) or magnetic resonance imaging (MRI) (Morales et al., 2004) using likewise edge-detection algorithms. There have been also attempts to reconstruct the circumference of tree rings in 3D (Morales et al., 2004; Laggoune et al., 2005) from MRI data. Although a 3D reconstruction was possible, the technique is limited by the sample size that can be placed within the device. Therefore, it would be difficult to effectively reconstruct an entire root system. Zu Castell et al. (2005) applied volume interpolations of CT images of a tree trunk based on differences in grey values of the CT images. Some of the typical problems occurred, such as the critical regions close to ring boundaries. The interpolation was dependent on the distance between slices and, thus, the number of slices. In some cases an overlay effect occurred, creating analyses errors that resulted in double rings or duplicated artifacts. But this effect could be reduced significantly by appropriate rotation of the slices.

If the reconstruction of entire ring structures in cross sections was realized, the resulting ring profiles would allow for more comprehensive analyses of roots and stems. Moreover, for scientists, to use the basal area increment to predict tree biomass, it is essential to know the entire structure of a specific ring.

In this study we develop a spatio-temporal 3D root growth model for which interpolated rings are crucial. We fully integrate entire tree-ring structures into a 3D coarse root model. This will be the basis for an annually resolved 3D root-growth model enabling a representation of the state of the root system for every year of its development.

Two data sets are required to fulfill this task: 2D ring-width data acquired with dendrochronological standard techniques and a 3D model of a root acquired via laser scanning (FARO ScanArm).

This paper continues the work presented in Wagner et al. (2010), where ring-width data of 4 radii of a cross section were integrated into a 3D surface model, acquired with a laser scanner at the corresponding positions to those in reality. We now concentrate on (i) the interpolation of the ring structures between the measured radii (in general 4 per cross section) and their integration into a 3D surface model of coarse roots, and (ii) the evaluation of the accuracy of the interpolation algorithm used and the review of its usefulness as a basis for a 3D root-growth model.

2. Methods

The presented approach is based on two independent data sets. One is a 3D laser-scan of the root structure and the other is a 2D ring-width data set representing the annual increment at defined cross sections. So far we have only used root segments, but our intention is to extend the approach to an entire root system. For the first interpolations, roots of Scots pine (*Pinus sylvestris* L.) and common ash (*Fraxinus excelsior* L.) were used, although the species is generally not important as long as annual growth rings are formed.

2.1. Laser scanning

In order to acquire the outer shape of a root segment, the structure of the root segment was acquired with the Faro laser ScanArm (FARO Technologies Inc., 2010). For this study, the scan device was equipped with a FARO laser line probe projecting the laser beam as a line on the surface of any object (Wagner et al., 2010). While emitting the beam line, an integrated camera takes a picture of the shape and the exact position of the line on the surface of the scanned object registering $x/y/z$-coordinates along the line (FARO Technologies Inc., 2010). Hence, the Faro scanning technique can be described as distance determination by optical triangulation. Resulting point clouds are cleared from noise and triangulated as described in Wagner et al. (2010).

2.2. Ring-width measurements

Before the surface was scanned, the corresponding positions for ring-width measurements were marked with pins (Bert and Danjon, 2005). Discs were then cut out of the root at this position perpendicular to the root axis to analyze the annual growth of the root segment. Afterwards the discs were sanded to ensure a plane surface. On each disc, ring widths were measured along four radii according to standard dendrochronological techniques (Cook and Kairiukstis, 1990) using the software WinDENDRO (Regent Instruments Inc., 2004). In general, the single radii were positioned perpendicular to each other. However, in some cases it was not possible due to deformations or cracks, so the angles had to be modified. WinDENDRO enables measuring ring-width variations based on scanned images of the polished discs generated by a distortion-free flatbed scanner. The output data of WinDENDRO were measured distances (ring widths) provided as

Table 1
Comparison of the descriptive statistics for measured and interpolated ring-width data (CS 1–5: cross sections 1–5).

	Mean (mm)	Stand Dev (mm)	Variance	Min (mm)	Max (mm)	No rings
CS 1						
Measured (O)	0.7756	0.1364	0.0264	0.2690	1.9030	13
Interpolated (*P*)	0.7774	0.1016	0.0142	0.2960	1.7669	13
CS 2						
Measured (*O*)	0.7269	0.1300	0.0255	0.2760	1.9410	13
Interpolated (*P*)	0.7211	0.0960	0.0141	0.3331	1.7116	13
CS 3						
Measured (*O*)	0.7036	0.1912	0.0469	0.2100	1.6130	13
Interpolated (*P*)	0.7013	0.1753	0.0413	0.2845	1.7825	13
CS 4						
Measured (*O*)	0.6489	0.1408	0.0265	0.1940	1.9900	13
Interpolated (*P*)	0.6527	0.1046	0.0158	0.2024	1.8310	13
CS 5						
Measured (*O*)	0.3182	0.1067	0.0154	0.0350	1.1740	30
Interpolated (*P*)	0.3235	0.0828	0.0096	0.0383	1.1416	30

text files. Descriptive statistics (Table 1) such as mean annual ring width, variance, standard deviation, minimum and maximum ring width were calculated to describe the tree-ring data (Fritts, 1976).

2.3. Reconstructions of tree-ring profiles

The goal of the interpolation procedure was to reconstruct entire ring profiles within a 3D root model, this allowed for estimations of ring-width at any point within a cross section and, at a later stage, at any point within a 3D model of tree roots. To compute such estimations the ring-width data from WinDENDRO needed to be integrated into the 3D model acquired with laser scanning (Wagner et al., 2010). This presented paper is based on this former model and concentrates on the reconstruction of the ring-profiles. As described in Wagner et al. (2010) an automated procedure to integrate the ring-width data into the 3D model was designed and implemented. The state after this integration is schematically shown in the lower right corner of the model in Fig. 1A. The ring-width measurements were brought back into a spatial context within the 3D model and hence, the corresponding positions to those in reality. Starting from this model, a new automated procedure to reconstruct entire ring structures was designed and implemented in MATLAB. This procedure allows retrieving the ring width on any arbitrary radius within the cross section. The reconstruction algorithm considered the outer shape of the 3D model retrieved via laser scanning as well as the data of the four radii measured in WinDENDRO. Hence, the input data for the reconstruction of ring profiles was four ring-width radii per cross section, which were already integrated into the 3D model (Wagner et al., 2010) along with the scan data representing the circumference of the corresponding cross section. The outer shape of each cross section was retrieved manually using the software Geomagic Studio 11 and, thus, cut out of the virtual 3D model. The circumference likewise consisted of several data points. On this basis we wanted to compute estimations of the ring-width distances for an arbitrary radius x (r_x) positioned between two input radii for which the actual ring-width distances were available. As an example, Fig. 2 shows

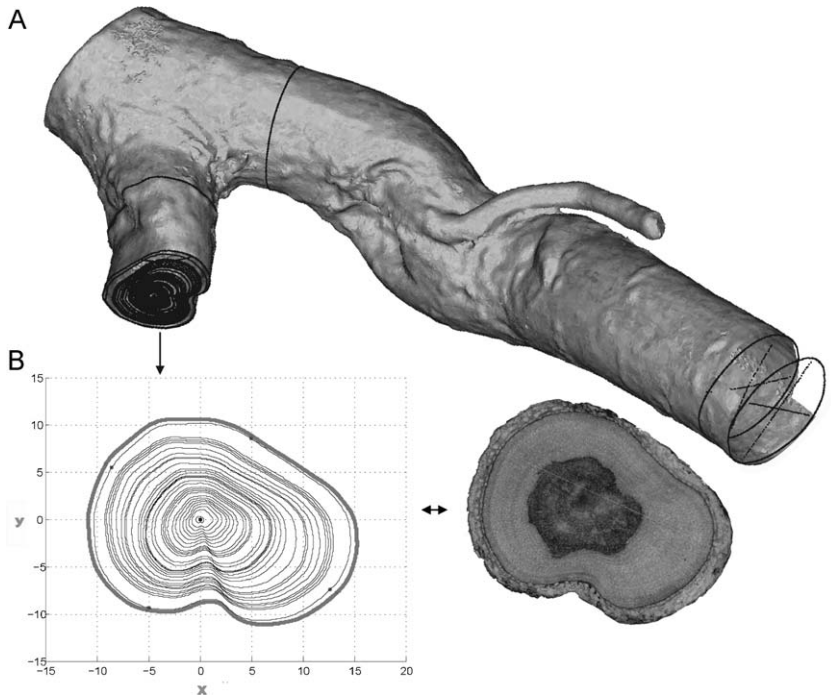

Fig. 1. (A) Integrated ring-width data along four radii and state of the model before ring interpolation were implemented (right side); integrated ring structures (left side). (B) The scan image of the cross section CS 5 (right side) and the corresponding interpolated ring structures (left side).

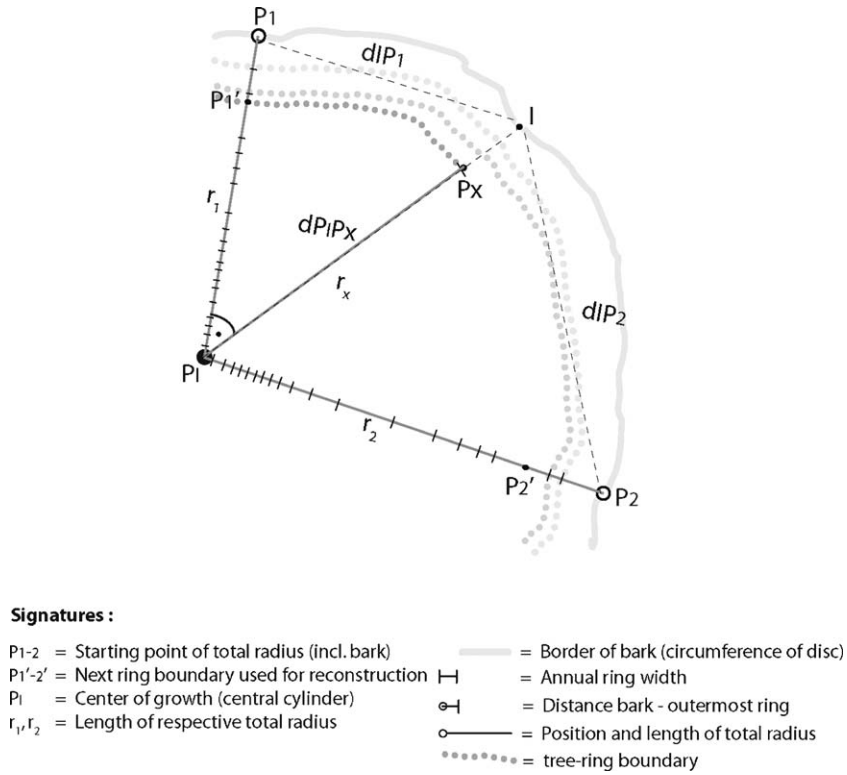

Fig. 2. Schematic view of the interpolation approach including parameters used.

the approach used for the sector between two input radii, here referred to as radius 1 (r_1) and radius 2 (r_2). The angle between r_1 and r_x, which is the radius of the new ring, is referred to as α. As a preliminary step, the corresponding intersection point (I) between the circumference of the cross section and the line going through the growth center (P_I) was calculated starting from r_1 in 1° steps (Fig. 2), although other arbitrary values for the angular steps could be chosen. Therefore, the following distances were computed (Fig. 2):

dIP_1; dIP_2: Distance between I and the starting point of r_1 at bark side (P_1 (P_2)), which gives a measure of the distance of r_x from r_1 (r_2).
dP_IP_1; dP_IP_2: Distance between the P_I and the P_1 (P_2).
dP_II: Distance between P_I and I.
dP_IP_1'; dP_IP_2': Distance between P_I and P_1' (P_2'), corresponding to the distance between P_I and the ring on r_1 (r_2), which is the next ring boundary to be reconstructed.
dP_IP_x: Distance between the P_I and the point P_x on r_x

In order to calculate the unknown distance from the center to P_x (dP_IP_x), the following ratios were considered:

$$\text{ratio}_1 = \frac{dP_IP_1'}{dP_IP_1}$$

$$\text{ratio}_2 = \frac{dP_IP_2'}{dP_IP_2}$$

$$\text{ratio}_x = \frac{dP_IP_x}{dP_II}$$

The ratio_1 (ratio_2) gave a measure of the distance of a specific tree ring to the bark with respect to the total length of r_1 (r_2). ratio_x represented the corresponding measure for the same tree ring, but in reference to r_x. Since dP_II was calculated, computing r_x directly allowed retrieving an approximation of the distance dP_IP_x.

Ratio_x could be computed considering the available information, under the assumption that the closer I is to P_1 (P_2) the closer the ratio_x should be to ratio_1 (ratio_2). Therefore, the following weight w_1 was designed:

$$w_1 = \frac{dIP_1}{dIP_1 + dIP_2}$$

Based on this ratio_x (see above) can be computed:

$$\text{ratio}_x = \text{ratio}_1 \cdot (1 - w_1) + \text{ratio}_2 \cdot w_1$$

Hence, if I coincided with P_1 then w_1 was zero and ratio_x would be equal to ratio_1. Alternatively, the higher the distance between I and

Table 2
Error performance for measured and interpolated tree-ring data (Sum of Square Errors (SSE), the Root Mean Square Error (RMSE) and the Mean Absolute Error (MAE)).

	SSE	RMSE	MAE	Correlation Coeff	p-Value
CS 1	0.3306	0.0837	0.0628	0.9932	1.2311e−011
CS 2	0.2941	0.0800	0.0610	0.9976	3.8771e−014
CS 3	0.3343	0.0878	0.0645	0.9952	1.9641e−012
CS 4	0.3518	0.0838	0.0630	0.9904	8.4893e−011
CS 5	0.3437	0.0855	0.0614	0.9783	1.0812e−020

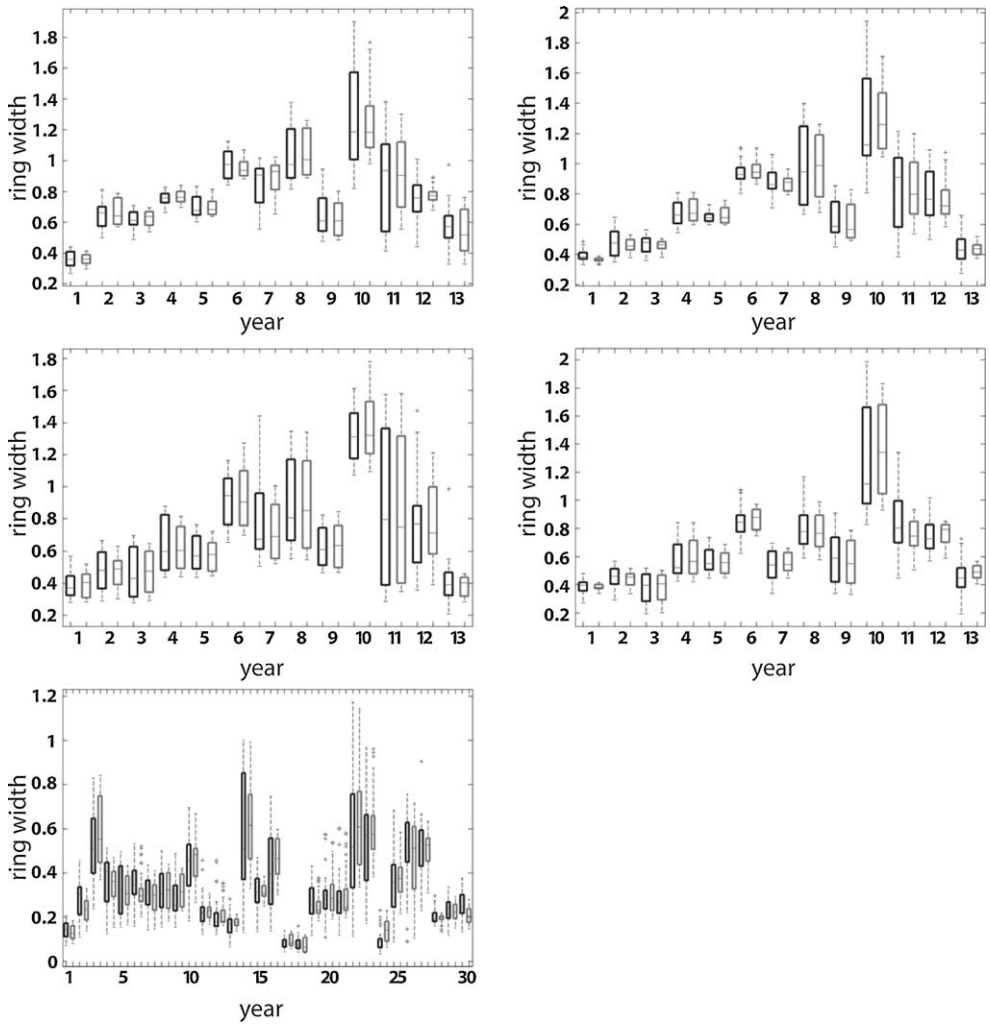

Fig. 3. Box plots for ring-width data per year comparing measured to interpolated data for cross sections 1–5. Column numbers do represent the annual rings of the respective cross sections, starting from the innermost ring (1 = year one, measured ring width (black); 1 = year one, interpolated ring width (grey); etc.).

P_1 (and, thus, the closer the distance of I to P_2) became, the lower the contribution of ratio$_1$ to the value of ratio$_x$ and the higher the correspondent contribution of ratio$_2$ would become.

2.4. Model performance and error computation

As a control for the accuracy of the resulting interpolated rings, 32 additional radii were measured on each cross section. Starting at one of the four main radii, every 10° a new radius was measured using WinDENDRO software resulting in a total of 36 measured radii per section. A separate MATLAB program was written to calculate 32 congruent radii every 10th degree, i.e. being calculated on the same position as the measured ones based on the interpolated ring data between the four main radii. To finally define the error values for each single interpolated ring, several error predictors were calculated. Among them are the Sum of Square Errors (SSE), the Root Mean Square Error (RMSE) and the Mean Absolute Error (MAE).

Equation (1) (e_i) calculates the individual model-prediction errors, where (P_i; $i = 1,2, \ldots, n$) are the interpolated values and (O_i; $i = 1,2, \ldots, n$) the measured values. The measure of average error (=model performance) is then based on statistical summaries of e_i ($i = 1,2, \ldots, n$) being part of SSE (Eq. (2)). Error values are the residuals of modelled and true ring-width data. Hence, the RMSE is the standard deviation of the error values of ring-width data of the cross sections. Since Willmott and Matsuura (2005), among others, stated that SSE and RMSE alone might not be reliable predictors for the average error, the mean absolute error (MAE) was additionally calculated (Eq. (4)).

$$e_i = P_i - O_i \tag{1}$$

$$\mathrm{SSE} = \sum_{i=1}^{n} |e_i|^2 \tag{2}$$

$$\mathrm{RMSE} = \left[n^{-1} \sum_{i=1}^{n} |e_i|^2 \right]^{1/2} \tag{3}$$

$$\mathrm{MAE} = \left[n^{-1} \sum_{i=1}^{n} |e_i| \right] \tag{4}$$

Pearson's correlation was performed to verify the results of the interpolation techniques and calculate the correlation between measured and interpolated data sets (Table 2).

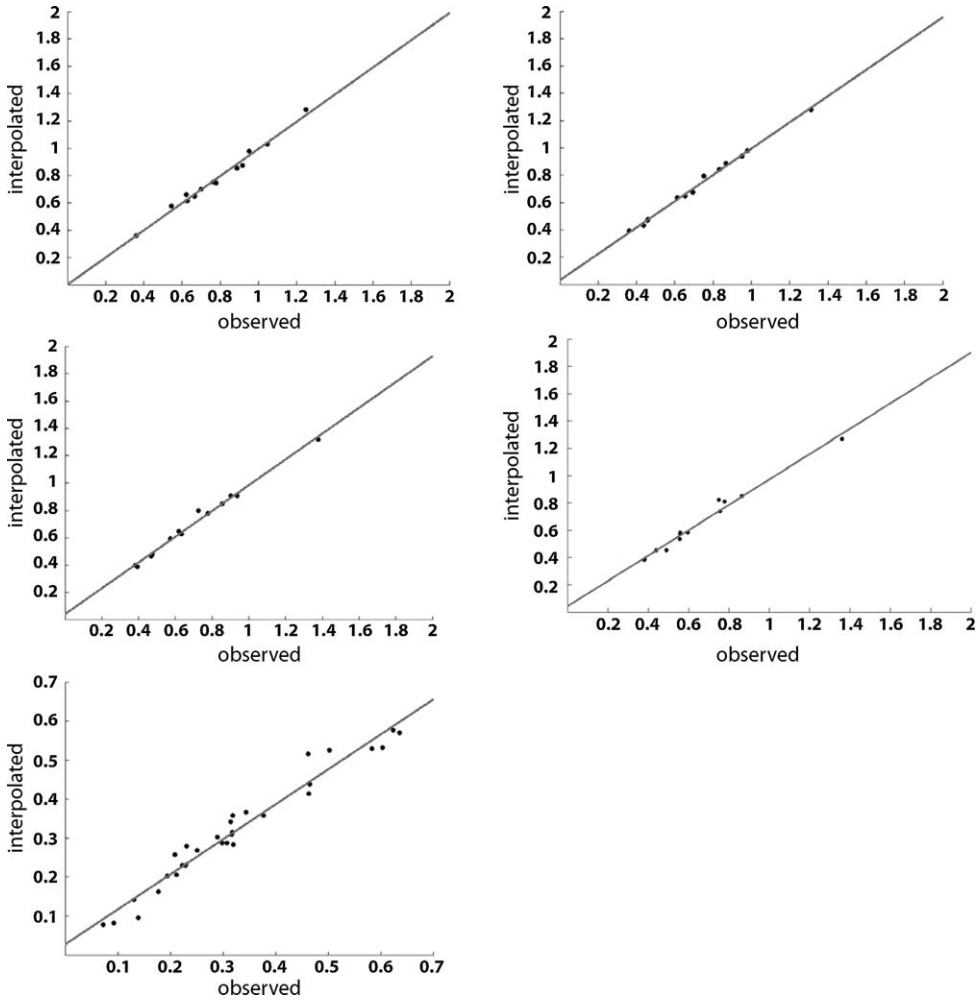

Fig. 4. The measured tree-ring data are plotted against the interpolated ring data for CS 1–5.

3. Results

3.1. Interpolation of rings

The interpolation of entire ring structures into the 3D surface model of a root segment was successfully implemented using a weighted interpolation algorithm. Hence, ring data was set into a spatial context (Fig. 1A) corresponding to those in reality. Fig. 1B shows the respective cross sections with reconstructed ring profiles.

3.2. Ring-width data

Table 1shows the descriptive statistics for the measured and the respective interpolated tree-ring data. The results show the high variability of the real ring data along a cross section, which can be observed in the variance and standard deviation of measured values in Table 1. The variance and standard deviation of the interpolated ring data of the same cross sections are comparable to the real measurements (Tables 1 and 2). This can also be visually observed in the box-plot diagram (Fig. 3). Interestingly, the standard deviation and variance is generally higher for the measurements compared to the interpolated values (Table 1). The mean ring width per cross section conforms also between measured and interpolated data. All values deviated less than 0.01 mm for all cross sections. Minimum and maximum ring-width was comparable for both data sets.

3.3. Measure of interpolation performance

MAE (Mean absolute error) was about 0.06 mm for all sections (Table 2). The agreement of data sets was verified by using Pearson's correlation (Table 2). In all sections, the correlation coefficient was above 0.9 and *p*-values were highly significant due to the dependence of data sets. Fig. 4 shows measured and interpolated data plotted against each other.

In Fig. 5, mean ring-width series of the 36 measured radii per cross section were plotted against the mean series of the 36 interpolated radii. The corresponding curves showed the same course, although a slight offset occurs in some cases.

For a more detailed picture, Fig. 6 focuses on single radii. The corresponding radii of measured versus interpolated were plotted against each other, but due to the large amount of data, only one cross section (CS 3) is shown. CS 3 was chosen, because it shows the biggest MAE among the five sections. Nevertheless, the radii series display the same general trend with a relatively small offset between curves. An exceptional case was ring 7, where a larger deviation occurred. In addition, CS 5 demonstrated rare cases of amplified deviations (Fig. 6). For all that the interpolated of CS 5 mean series reconstructed the measured series in a convincing way.

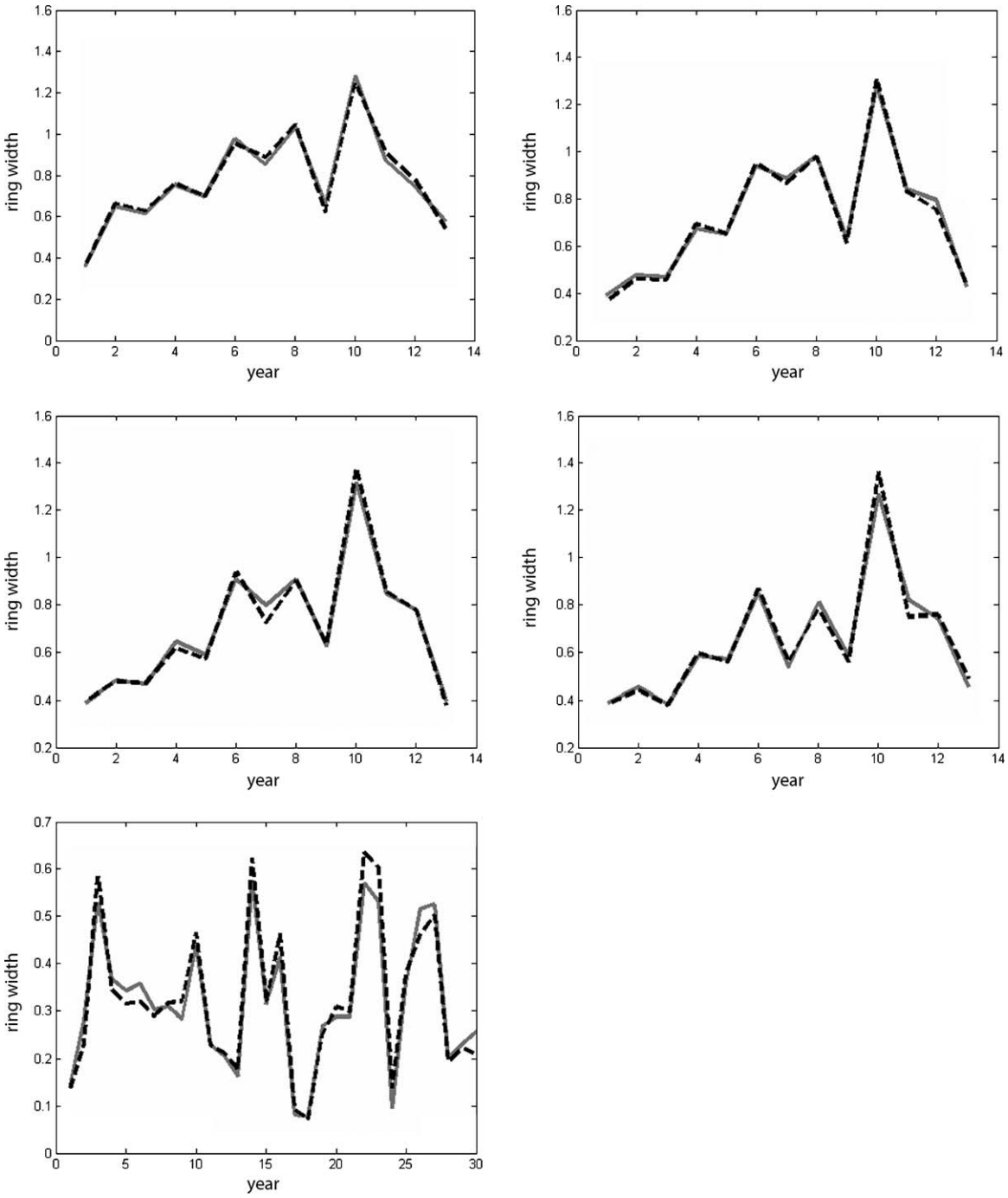

Fig. 5. Mean tree-ring series of measured rings (grey) plotted against interpolated ring data (dashed, black) of CS 1–5 (*x*-axis number of years; *y*-axis ring width).

4. Discussion

The approach presented is able to interpolate the ring structures between 4 radii of a cross section in dependence on the ring-width data. The reliability of this method to accurately model the reality is of great interest and should be investigated, since it promises as valuable tool to support or even replace manual tree-ring measurements on cross sections for more comprehensive analyses. Another query posed by this study is whether the interpolations are accurate and affirm basis for ongoing 3D interpolations of an entire 3D root-development model.

As expressed in the variance and standard deviation of Table 1 and the box plots (Fig. 3), ring-width variations were evidently high throughout cross sections. This was true in terms of year to year variability, as well as for the ring-width variation within a specific year along the cross section (Fig. 3).

Hence, if the accuracy of the presented data is to be judged, one should consider that tree-ring data is inherently highly variable. Therefore, MEA of 0.06 mm seems to be a rather convincing result. However, depending on the ring width it can be a quite huge percentage of narrow rings. Causes for deviations between measured and interpolated data can also be due to measurement error and

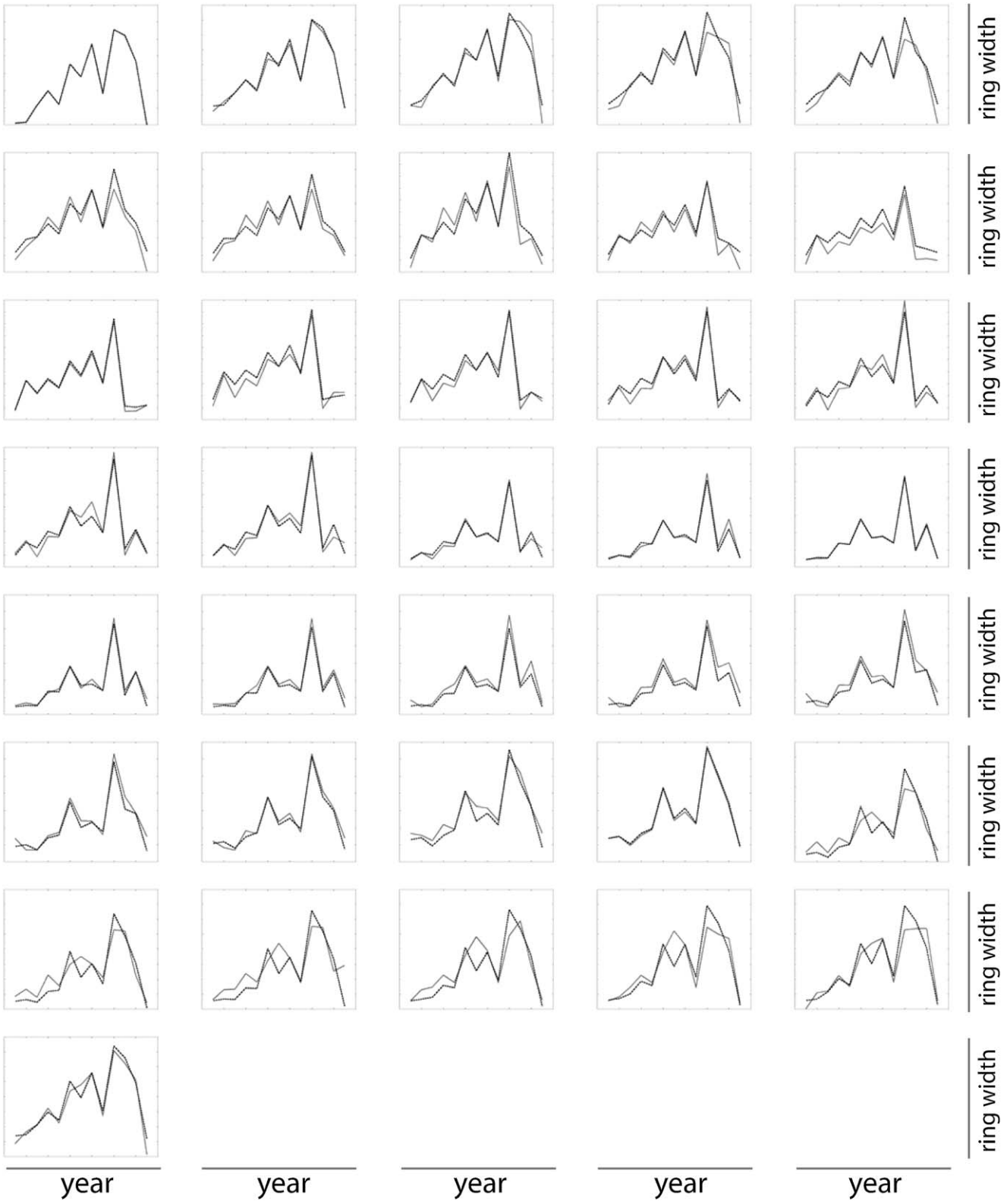

Fig. 6. Measured series (grey) plotted against interpolated series (dashed, black) for single radii (1–36) of CS 3 (*x*-axis number of years; *y*-axis ring width).

not just a result of interpolations. Even though tree-ring measurements themselves are highly accurate, deviations can occur from measurement to measurement and between measurers. In some tree-ring laboratories ring cores are measured by different persons as a performance control. If deviations above 0.1 mm per ring occur, data are controlled again (Fritts, 1976). Hence, every deviation below 0.1 mm is accepted as a neglectable measurement error. The deviations in this study were on average below this range and given this the results are considered a reliable approximation of reality.

Moreover, mean chronologies of the interpolated data sets demonstrated accurate reproducibility of measured mean chronologies (Fig. 4). With respect to radii chronologies, most results were also convincing and their curves show the same growth patterns, with slight offsets (Fig. 4). However, some of the radii (e.g., radii of CS 5) showed a stronger deviation resulting also in higher deviations of the mean chronology (Fig. 5). Possible explanations are (I) extreme differences between inner rings and the circumference of the section, (II) extremely deformed sections, or (III) abrupt growth changes between the adjacent radii.

Cerda et al. (2007) made the assumption that all rings can be obtained by scaling the shape of the bark. If the bark represents the shape of the outer ring accurately approximations are considered good, which is confirmed by their results. However, shapes within the section can vary significantly from the outer shape of the bark, and generated problems for Cerda et al. (2007). If higher deviations occur, the inclusion of the ring-width data is able to partially compensate for deviations due to shape. Thus, the weighted interpolation algorithm presented in this study used both data sets, the outer shape of the section and the variation of the 4 radii. In doing so, the deviations were compensated for. In general, this seems to allow for reliable reconstructions of the rings.

As can be seen in Table 1 interpolated ring structures had a generally lower variance and standard deviation than measured values, which can be attributed to the weighted interpolation algorithm applied. For a case of abrupt growth changes between measured radii and therefore, stronger deviations between inner ring structures and the outer bark shape, the algorithm might not be able to reconstruct this extreme growth changes in a realistic way and smooth the shape. Given this the reconstruction of extreme deformations (e.g., caused by injuries) with a high accuracy would generate a disproportional workload. Since these disturbances are in general restricted to small areas their reconstruction would not provide additional gain for the overall results. In individual cases, it might be necessary to measure additional radii on the specific cross section and thus, base interpolations on 5 rather than 4 input radii (Wagner et al., 2010). However, in general 4 radii per cross section was a realistic workload. The results confirm this to be sufficient for interpolations. For species with an irregular bark, it might be necessary to smooth the triangulated surface of the 3D root model in Geomagic software before interpolating the ring structures.

However, these cases are exceptions and a control function will be integrated into the program to filter these cases. For a cross section where interpolations deviate more than 0.1 mm, a program error will occur and a data check is requested.

Although cross section 5 was quite deformed (Fig. 1B), it was possible to interpolate the ring structures with a MAE of 0.0614 and the mean chronologies showed a common pattern. Hence, these results highlight the successful implementation of the algorithm and thus we are convinced that a reliable base was implemented for 3D interpolations. However, if specific reactions of trees are to be analyzed, some curves should be taken with caution and additional analyses might be needed.

5. Conclusion and outlook

The basis for more comprehensive ring-width studies within a root system was successfully implemented due to the successful integration and interpolation of tree-rings into the 3D surface model. Interpolations are always approximations to reality. The results presented here are promising approximations and within a good prediction range. Therefore, these data are a useful basis for a 3D root-growth model, which mark the overall aim of ongoing studies. For the finalisation, growth layers, representing the single growth years of the root between single cross sections, will be interpolated in a next step. For every single growth year a closed surface will be generated, which allows for a 3D reconstruction of root development over time, annual biomass acquisition and more comprehensive ring-width analyses. Hence, the presented results are the indispensable premise for a 3D root model.

Automatic detection of ring structures might be a future task and computer scientists are already working to improve these techniques. So far the programs available on the market are not reliable enough, which makes manual measurement necessary. However, if reliable techniques become available, the presented model can be adapted. In the future, image analyses approaches might reach a stage where ring structures can be automatically detected independently of species without problems. However, so far this stage has not yet been reached, and hence still a close collaboration between image analyses and application experts is required (Soille and Misson, 2001).

For the acquisition of the entire structure of a root system and for ring measurements of roots, it will always be necessary to excavate the tree in order to gain root cross sections for ring measurements. In order to model root structure this is also true for our approach, since reliable non-destructive techniques are not yet available for 3D acquisition. However, if the presented interpolations are transferred to the above-ground part of a tree on the basis of 4 cores it will be possible to simulate the interior of trees without cutting the tree down. The aboveground tree shape could be acquired with a terrestrial laser scanner in the stand. This will make the program a useful tool for volume computations of single trees within stands, which is an important task for foresters in terms of wood productivity and for the acquisition of biomass.

Acknowledgements

The authors wish to thank the Swiss National Science Foundation (SNF) for funding the project (No.: 200021-113450). Furthermore, the authors are grateful to Dr. Ingo Heinrich for helpful comments on the final version of the manuscript.

References

Bert, D., Danjon, F., 2005. Carbon concentration variations in the roots, stem and crown of mature *Pinus pinaster* (Ait.). Forest Ecology and Management 222, 279–295.

Bindzi, I., Samson, M., Kamoso, L.M., 1996. Modélisation géométrique d'une bille de bois. Annals of Forest Science 53, 21–30.

Cerda, M., Hitschfeld-Kahler, N., Mery, D., 2007. Robust tree-ring detection. In: Mery, D., Rueda, L. (Eds.), PSIVT 2007, LNCS, vol. 4872. Springer, Heidelberg, pp. 575–585.

Conner, W.S., Schowengerdt, R.A., Munro, M., Hughes, M.K., 1998. Design of a computer vision based tree ring dating system. In: IEEE Southwest Symposium on Image Analysis and Interpretation , Tucson, AZ, USA, pp. 256–261.

Conner, W.S., Schowengerdt, R.A., Munro, M., Hughes, M.K., 2000. Engineering design of an image acquisition and analysis system for dendrochronology. Optical Engineering 39, 453–463.

Cook, E.R., Kairiukstis, L.A. (Eds.), 1990. Methods of Dendrochronology. Applications in the Environmental Sciences. Kluwer, Dordrecht, 394 pp.

Danjon, F., Reubens, B., 2008. Assessing and analyzing 3D architecture of woody root systems, a review of methods and applications in tree and soil stability, resource acquisition and allocation. Plant and Soil 303, 1–34.

Entacher, K., Planitzer, D., Uhl, A., 2007. Towards an automated generation of tree ring profiles from CT-images. In: Petrou, M., Saramäki, T., Ercil, A., Loncaric, S. (Eds.), Proceedings of the 5th International Symposium on Image and Signal Processing and Analysis (ISPA'07). Istanbul, Turkey, pp. 174–179.

Fablet, R., Le Josse, N., 2005. Automated fish age estimation from otholith images using statistical learning. Fisheries Research 72, 279–290.

FARO Technologies Inc., 2010. http://www.faro.com/.

Fritts, H.C., 1976. Tree Rings and Climate. Academic Press, London, 567 pp.

Geomagic Studio 11.0, 2009. Available in http://www.geomagic.com/en/products/.

He, Z., Munro, M.A.R., Gopalan, G., Hughes, M.K., 2008. System and algorithm design for a new generation tree-ring image analysis system. Optical Engineering 47, 027003-1–027003-15.

Heuret, P., Meredieu, C., Coudurier, T., Barthélémy, D., 2006. Ontogenetic trends in the morphological features of main stem annual shoots of *Pinus pinaster* (Pinaceae). American Journal of Botany 93, 1577–1587.

Ikami, Y., Matsumura, Y., Murata, K., Tsuchikawa, S., 2008. Estimation of sawn face width of Sugi (*Cryptomeria japonica* D. Don) logs by cross-sectional shape with approximation profile. Holz als Roh- und Werkstoff 66, 243–247.

Laggoune, H., Sarifuddin, Guesdon, V., 2005. Tree ring analysis. In: Canadian Conference on Electrical and Computer Engineering , Saskatchewan, Canada, pp. 1574–1577.

Le Blanc, D.C., 1990. Relationships between breast-height and whole-stem growth indices for red spruce on Whiteface Mountain, New York. Canadian Journal of Forest Research 20, 1399–1407.

Lewis, K.J., 1997. Growth reduction in spruce infected by *Inonotus tomentosus* in central British Columbia. Canadian Journal of Forest Research 27, 1669–1674.

Longuetaud, F., Mothe, F., Leban, J.-M., 2007. Automatic detection of the heartwood/sapwood boundary within Norway spruce (*Picea abies* (L.) Karst.) logs by means of CT images. Computers and Electronics in Agriculture 58, 100–111.

Mattheck, C., Breloer, H., 1995. The Body Language of Trees. A Handbook for Failure Analysis. HMSO, London, 320 pp.

Morales, S., Guesalaga, A., Fernández, M.P., Guarini, M., Irarrázaval, P., 2004. Computer reconstruction of pine growth rings using MRI. Magnetic Resonance Imaging 22, 403–412.

Regent Instruments Inc., 2004. WinDENDRO: Tree Ring, Stem, Wood Density Analysis and Measurement. Regent Instruments Inc., Quebec City, Canada.

Saint-André, L., 1998. Excentricité et forme des sections transversales de bois. Définitions, méthodologie, exemples sur l'épicéa commun (*Picea abies* Karst.). Annals of Forest Science 55, 899–909.

Saint-André, L., Leban, J.-M., 2000. An elliptical model for tree ring shape in transverse section. Methodology and case study on Norway spruce. Holz als Roh- und Werkstoff 58, 368–374.

Schweingruber, F.H., 2007. Wood Structure and Environment. Springer Series in Wood Science. Springer, Heidelberg, 279 pp.

Skatter, S., 1998. Determination of cross-sectional shape of softwood logs from three x-ray projections using an elliptical model. Holz als Roh- und Werkstoff 56, 179–186.

Skatter, S., Høibø, O.A., 1998. Cross-sectional shape models of Scots pine (*Pinus silvestris*) and Norway spruce (*Picea abies*). Holz als Roh- und Werkstoff 56, 187–191.

Soille, P., Misson, L., 2001. Tree ring area measurements using morphological image analysis. Canadian Journal of Forest Research 31, 1074–1083.

Speer, J.H., 2010. Fundamentals of Tree-ring Research. The University of Arizona Press, Tucson, Arizona, 368 pp.

von Arx, G., Dietz, J., 2005. Automated image analysis of annual rings in the roots of perennial forbs. International Journal of Plant Sciences 166, 723–732.

Wagner, B., Gärtner, H., Ingensand, H., Santini, S., 2010. Incorporating 2D tree-ring data in 3D laser scans of coarse root systems. Plant and Soil 334, 175–187.

Wigley, T.M.L., Briffa, K.R., Jones, P.D., 1984. On the average value of correlated time series, with applications in dendroclimatology and hydrometeorology. Journal of Applied Meteorology 23, 201–213.

Willmott, C.J., Matsuura, K., 2005. Advantages if the mean absolute error (MAE) over the root mean square error (RMSE) in assessing average model performance. Climate Research 30, 79–82.

Zu Castell, W., Schrödl, S., Seifert, T., 2005. Volume interpolation of CT images from tree trunks. Plant Biology 7, 737–744.